Supplementary information to article: Viscoelastic characterization of cells at high-throughput in hyperbolic microchannels

Interfacial tension and droplet viscosity from hyperbolic channel measurements

In the main text, Equations (7)-(11) introduce a formalism how to calculate interfacial tensions and relaxation times from the Taylor deformation D_T of a droplet at a constant extension rate $\dot{\varepsilon}$. This introduces two equations ((8) and (11)) to compute the interfacial tension from the measurement parameters. By equating Equation (8) and (11), one can derive an equation to calculate the droplet viscosity η_{drop} from the extension rate, the viscosity of the carrier solution η_0, the droplet relaxation time τ, and the steady state deformation D_∞:

$$\frac{5\dot{\varepsilon}\tau}{D_\infty} = \hat{\eta}(2\hat{\eta}+3)$$

$$\Rightarrow 0 = \hat{\eta}^2 + \frac{3}{2}\hat{\eta} - \frac{5\dot{\varepsilon}\tau}{2D_\infty}$$

$$\Rightarrow \eta_{\mathrm{drop}} = \eta_0\left(\sqrt{\frac{9}{16}+\frac{5}{2}\frac{\dot{\varepsilon}\tau}{D_\infty}}-\frac{3}{4}\right). \qquad \text{(S1)}$$

D_∞ and τ result from an exponential fit to the deformation data (Equation (29)). The extension rate $\dot{\varepsilon}$ is derived from the droplet velocity curve. The interfacial tension can then be calculated with either Equation (8) or (11).

Derivation of hyperbolic channel profile

Equation (15) introduces the construction formula for the hyperbolic contraction with the aim of achieving a constant extension rate along the flow centerline. The centerline velocity is calculated according to Equation (14). The derivate $\partial u_0/\partial x$ reads:

$$\frac{\partial u_0}{\partial x} = \frac{3Q}{2H}\frac{1}{(w(x)-0.63H)^2}\cdot\frac{\partial w}{\partial x} \equiv \dot{\varepsilon}\,. \qquad \text{(S2)}$$

This leads to the following differentials:

$$\frac{2H\dot{\varepsilon}}{3Q}\mathrm{d}x = \frac{\mathrm{d}w}{w(x)-0.63H}\,. \qquad \text{(S3)}$$

With $A = \frac{2H\dot{\varepsilon}}{3Q}$, integration leads to the following relation:

$$w(x) = 0.63H - \frac{1}{Ax+C_1}, \qquad \text{(S4)}$$

With an integration constant C_1. By Fixing $w(0) = w_c$, one gets Equation (15) presented in the main text. At the contraction length L_c, Equation (15) becomes:

$$w(L_C) = w_u = 0.63H - \left(AL_c - \frac{1}{0.63H-w_c}\right)^{-1}. \qquad \text{(S5)}$$

Equation (S5) gives a general construction formula that defines a channel by fixing the parameters w_u, w_c, and L_c (Equation (16)). The expected extension rates result from the factor A by setting a flow rate and channel height.

Real-time deformability cytometry

The stiffness of PAAm beads used in this study was determined by measurements with real-time deformability cytometry (RT-DC). RT-DC was introduced in 2015 by Otto et al.[1] To determine the Young's modulus, we used the model described by Wittwer et al.[2] and viscosity model for the 0.6% MC-PBS from Büyükurgancı et al.[3]

In brief, we used the same AcCellerator setup (Zellmechanik Dresden) for the RT-DC measurements as for the experiments in hyperbolic channels. The microfluidic chip had a measurement region with a cross-section of 30×30 µm, where the deformed beads were recorded. The resulting Young's moduli for each bead type are shown in Figure S1 and the median Young's moduli are listed in Table S1.

Log-logistic growth function fit to Latrunculin B dose response curve

The Young's modulus data shown in Figure 5B was well described with a log-logistic growth function as proposed in Urbanska et al:[4]

$$E = E_{\mathrm{lower}} + \frac{E_{\mathrm{upper}} - E_{\mathrm{lower}}}{1+\exp\left(a\left[\ln\left(\frac{c_{\mathrm{LatB}}}{[\mathrm{nM}]}\right) - \ln\left(\frac{\mathrm{EC}_{50}}{[\mathrm{nM}]}\right)\right]\right)}. \qquad \text{(S6)}$$

with the LatB concentration, c_{LatB}, the lower bound, E_{lower}, and upper bound, E_{upper}, the steepness, a, and the effective EC_{50} dose at which half-maximum response is obtained. The resulting values for all flow rates are given in Table S4. The resulting EC_{50} values are in the range of 9-13 nM and in line with previous reports.[4,5]

References

1 O. Otto, P. Rosendahl, A. Mietke, S. Golfier, C. Herold, D. Klaue, S. Girardo, S. Pagliara, A. Ekpenyong, A. Jacobi, M. Wobus, N. Töpfner, U. F. Keyser, J. Mansfeld, E. Fischer-Friedrich and J. Guck, Real-time deformability cytometry: on-the-fly cell mechanical phenotyping, *Nat Methods*, 2015, **12**, 199–202.

2 L. D. Wittwer, F. Reichel, P. Müller, J. Guck and S. Aland, A new hyperelastic lookup table for RT-DC, *Soft Matter*, 2023, **19**, 2064–2073.

3 B. Büyükurgancı, S. K. Basu, M. Neuner, J. Guck, A. Wierschem and F. Reichel, Shear rheology of methyl cellulose based solutions for cell mechanical measurements at high shear rates, *Soft Matter*, 2023, **19**, 1739–1748.

4 M. Urbanska, H. E. Muñoz, J. Shaw Bagnall, O. Otto, S. R. Manalis, D. Di Carlo and J. Guck, A comparison of microfluidic methods for high-throughput cell deformability measurements, *Nat Methods*, 2020, **17**, 587–593.

5 R. Gerum, E. Mirzahossein, M. Eroles, J. Elsterer, A. Mainka, A. Bauer, S. Sonntag, A. Winterl, J. Bartl, L. Fischer, S. Abuhattum, R. Goswami, S. Girardo, J. Guck, S. Schrüfer, N. Ströhlein, M. Nosratlo, H. Herrmann, D. Schultheis, F. Rico, S. J. Müller, S. Gekle and B. Fabry, Viscoelastic properties of suspended cells measured with shear flow deformation cytometry, *Elife*, 2022, **11**, e78823.

Supplementary tables

Table S1: Characterization of PAAm beads. Short names show internal labels for different bead types. Diameters were measured by brightfield microscopy after production. Young's moduli were measured with RT-DC (see Fig. S1).

Short name	Total monomer concentration [$\%c_T$]	Diameter (mean ± SD) [µm] after production	Young's modulus (mean ± SEM) [Pa]
S4_12µm	4.5	12.7 ± 0.7	300 ± 2
S4_17µm	4.5	17.1 ± 0.6	379 ± 17
S4_18µm	5.2	18.7 ± 0.6	669 ± 32
S8_15µm	5.2	14.7 ± 0.8	832 ± 15
S0_3 Set 1	6.0	13.7 ± 0.4	1819 ± 77
S0_3 Set 2	6.0	14.5 ± 0.4	1846 ± 66
S0_3 Set 3	6.0	16.0 ± 0.4	1493 ± 17
S0_3 Set 4	6.0	16.6 ± 0.4	1347 ± 19

Table S2: Number of beads in the data for Figures 2C,F and S2E.

Bead type	**Flow rate [µL/s]**											
Youngs modulus [Pa]	0.01	0.02	0.03	0.04	0.05	0.06	0.07	0.08	0.09	0.10	0.12	0.14
300	377	552	754	1084	1404	1805	1624	1810	1882	1982	1680	1540
1347	-	190	285	360	451	493	-	667	-	792	691	453
1493	-	292	387	596	795	949	-	1053	-	1331	1540	1618

Table S3: Number of beads included in the data for Figures 2D,E and S2C,D.

Measurement region and Figure panels	**Bead type** Radius [µm] / $\boldsymbol{E}$ [Pa]	**Flow rate [µL/s]** 0.01	0.02	0.04	0.06	0.08	0.10
Inlet Figure 2D & S2C	5.5 / 300	-	786	781	806	785	749
	6.6 / 832	-	2966	4947	5853	5883	7863
	7.3 / 379	-	585	973	1951	2429	2429
	8.3 / 669	-	445	978	1969	2458	2944
Channel Figure 2E & S2D	5.5 / 300	764	792	761	770	757	714
	6.4 / 1819	984	989	993	989	991	995
	6.7 / 1846	991	983	986	988	987	984
	7.4 / 1493	981	984	986	981	968	966
	7.7 / 1347	102	214	461	483	487	494

Table S4: Fit values for the dose response of HL60 cells' Young's moduli as function of LatB concentration (Fig. 5B) fitted with equation S6.

Flow rate [µL/s]	$\mathbf{EC_{50}}$ [nM]	E_{lower} [Pa]	E_{upper} [Pa]	a
0.01	12.7 ± 3.9	80 ± 11	183 ± 7	1.5 ± 0.6
0.02	9.7 ± 1.4	136 ± 8	254 ± 8	3.5 ± 2.1
0.03	9.0 ± 1.5	210 ± 9	349 ± 10	3.3 ± 1.8

Table S5: Number of cells included in the HL60 + LatB data for Figures 5B-D and S7.

Date	Flow rate [µL/s]	LatB concentration [nM]								
		0	0.1	1	5	10	25	50	100	250
20230912	**0.01**	720	629	168	912	1433	1129	1514	1012	1121
	0.02	1068	1181	338	1366	1616	1593	1577	1674	1772
	0.04	2034	2104	711	2087	1880	1868	1894	1942	2087
20230914	**0.01**	750	675	1068	1403	1129	1597	1006	1310	1243
	0.02	1574	1331	1410	1565	1554	1569	1495	1541	1746
	0.04	1846	1877	1671	1829	1804	3129	1744	1866	2072
20230919	**0.01**	341	363	732	1082	901	577	474	798	682
	0.02	692	984	1414	1684	1670	1016	968	1530	1060
	0.04	2484	1409	1932	1905	2590	2036	1712	2379	1325

Table S6: Number of cells included in the HL60 + Nocodazole + LatB data for Figures 5E-G and S8.

Date	Flow rate [µL/s]	Sample			
		CTRL	LatB	Noco	LatB+Noco
20231010	**0.01**	839	922	832	643
	0.02	1491	1595	1515	1142
	0.04	1778	1994	1777	1935
20231012	**0.01**	1551	1748	1494	1957
	0.02	1414	1839	1394	2100
	0.04	1770	2304	1622	2535

Supplementary Figures

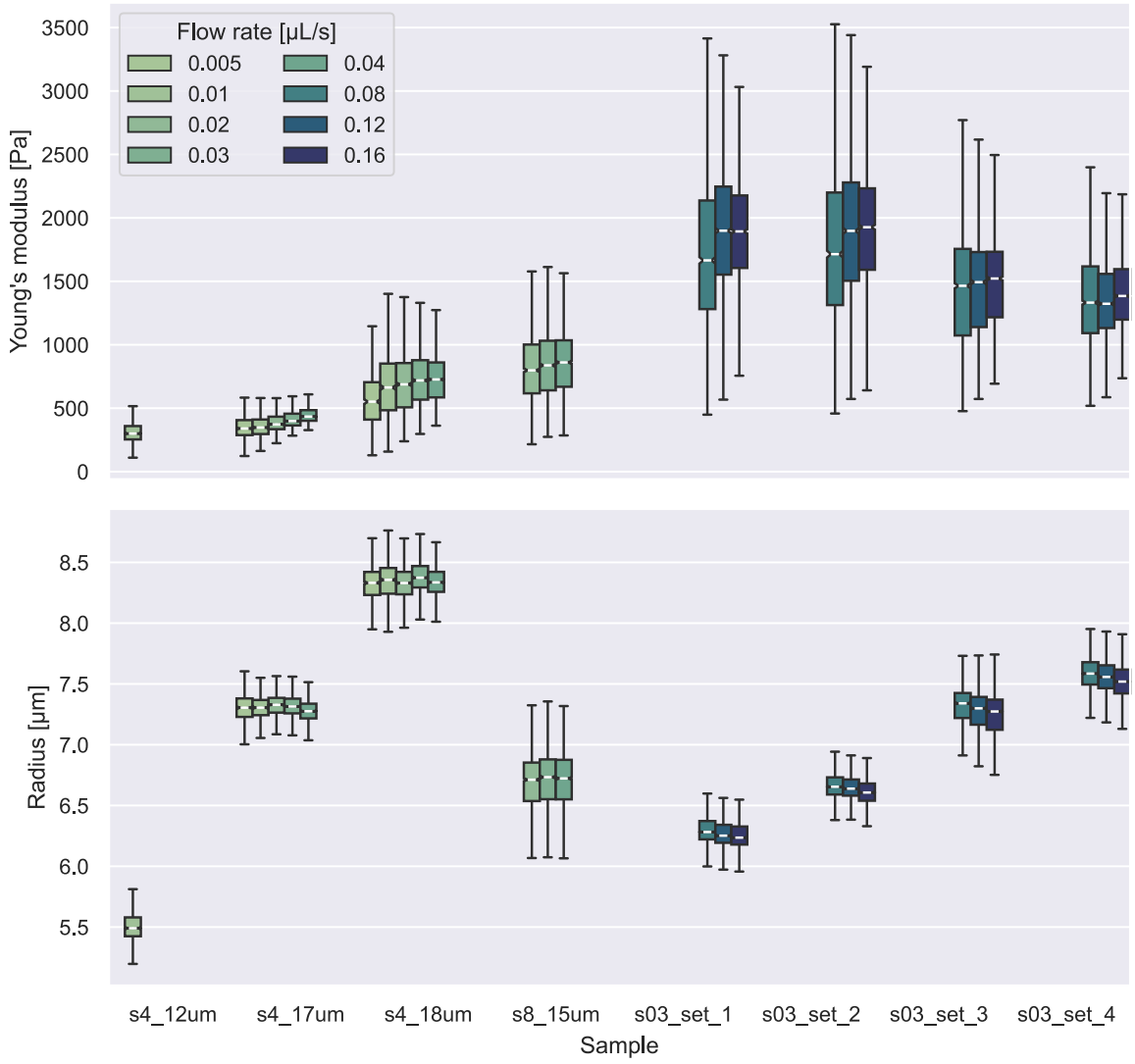

Figure S1: Young's moduli and radii of PAAm beads from RT-DC measurements. The radius was calculated from the measured volume, assuming the initial shape was a sphere. Boxes represent the inter-quartile range (IQR). Whiskers show 1.5×IQR borders. Notches around the median indicate the 95% confidence interval. Beads were measured at different flow rates because stiffer beads require higher flow rates to achieve the deformations for accurate computation of the Youngs'modulus.

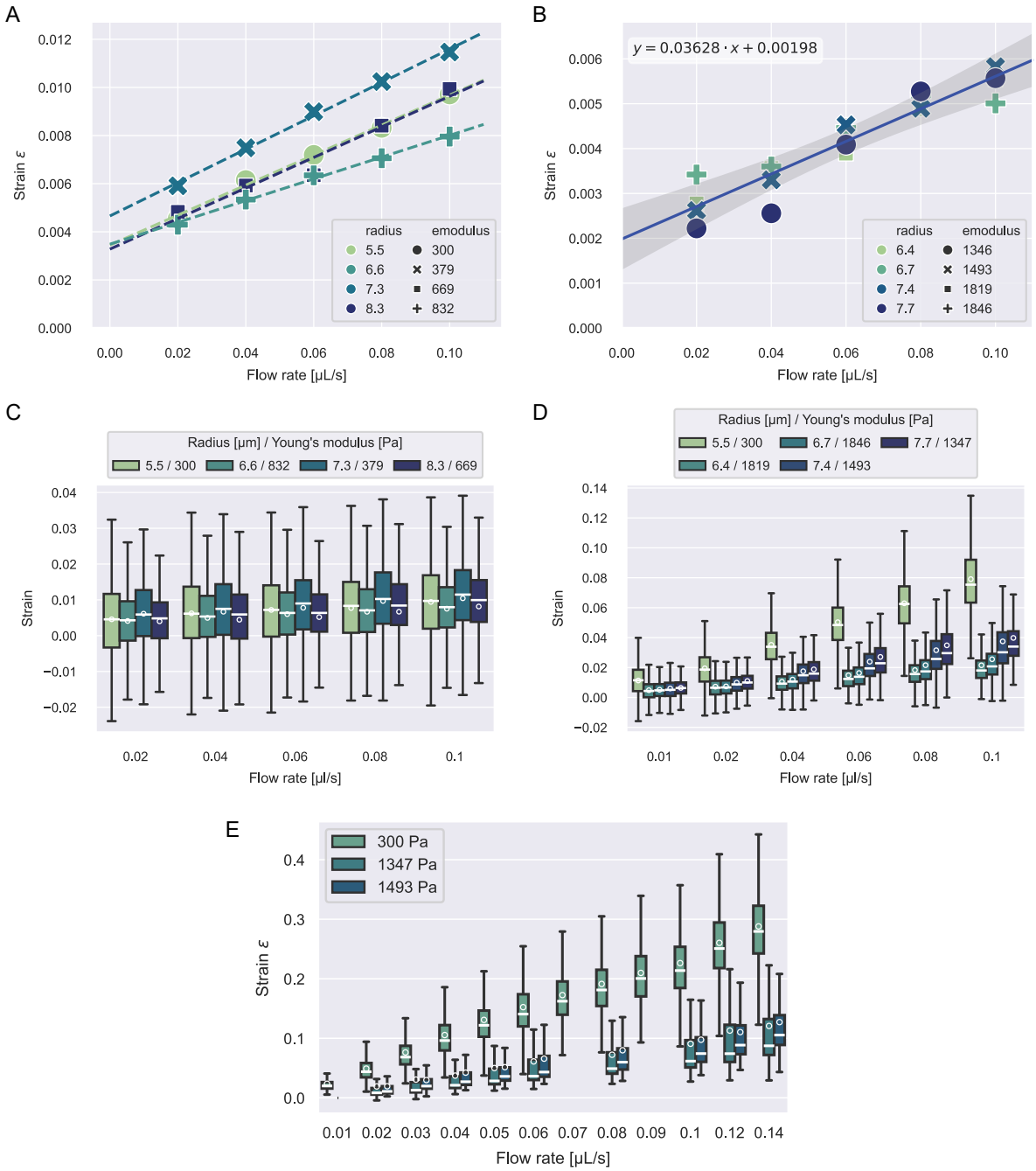

Figure S2: Strain correction for beads stress measurements (main text Fig. 2). The strain offset was determined by the intercept of a linear fit to the median strain data vs. flow rate measured in the inlet region. **A**) Strain data and linear fits for beads of type S4 or S8 (see Table S1). The resulting intercepts, ε_0, per bead Young's modulus are: $\varepsilon_0(300\ \mathrm{Pa}) = 0.0034$, $\varepsilon_0(379\ \mathrm{Pa}) = 0.0047$, $\varepsilon_0(669\ \mathrm{Pa}) = 0.0033$, $\varepsilon_0(832\ \mathrm{Pa}) = 0.0035$ **B**) Strain data and linear fit to the data for beads of type S03. For this bead type, we used the same correction for all samples. The solid line indicates the linear fit to all datapoints and the shaded gray area represents the 2-sigma error band. $\varepsilon_0(S03) = 0.00198$. **C**) Boxplots for strain data in main text Figure 2D. Boxes represent IQR and whiskers 1.5×IQR. White lines show medians and white circles means. **D**) Boxplots for strain data in Figure 2E. **E**) Boxplots for strain data in Figure 2C.

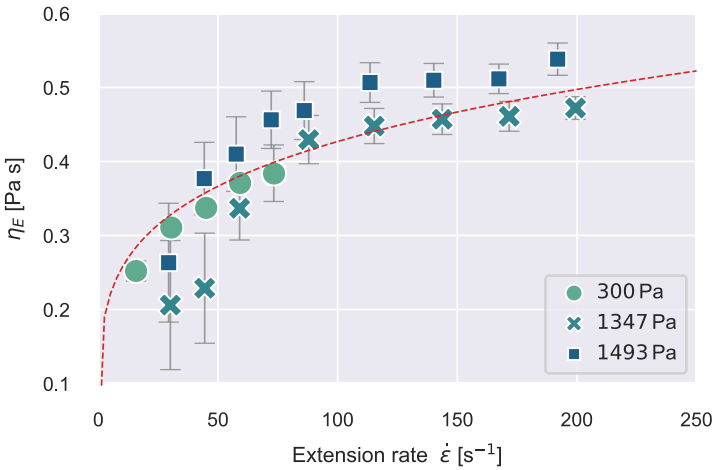

Figure S3: Extensional viscosity of 0.6% MC-PBS. Extensional viscosities for the data presented in Figure 2F. The red dashed line represents the power law in Equation (27) for the extensional viscosity: $\eta_E = 0.16\ (\dot{\varepsilon}/\dot{\varepsilon}_0)^{0.22}$.

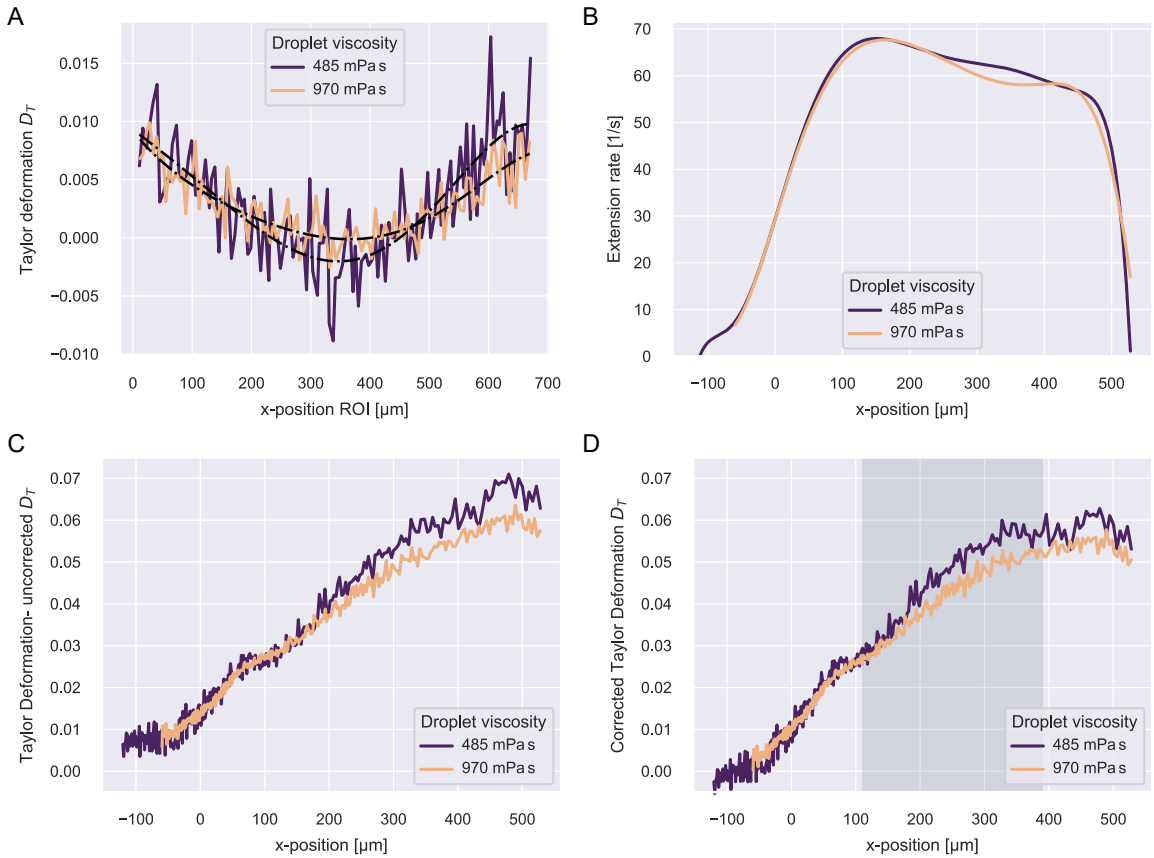

Figure S4: Strain correction and extension rate for measurements on silicone oil droplets. **A**) Taylor deformation as function of x in the inlet region of the channel at a flow rate of 0.01 µL/s. The black dash-dotted curves indicate a 6th order polynomial fit to the data. **B**) Extension rate as function of x in the hyperbolic region. **C**) Taylor deformation of the silicone oil droplets before correction. **D**) Corrected Taylor deformation as function of x in the hyperbolic region. The shaded region indicates the analysis region to compute relaxation times, interfacial tension and droplet viscosity that is used in Figure 3. The curve was generated by the data in C, subtracting the values resulting from the polynomial fit shown in A.

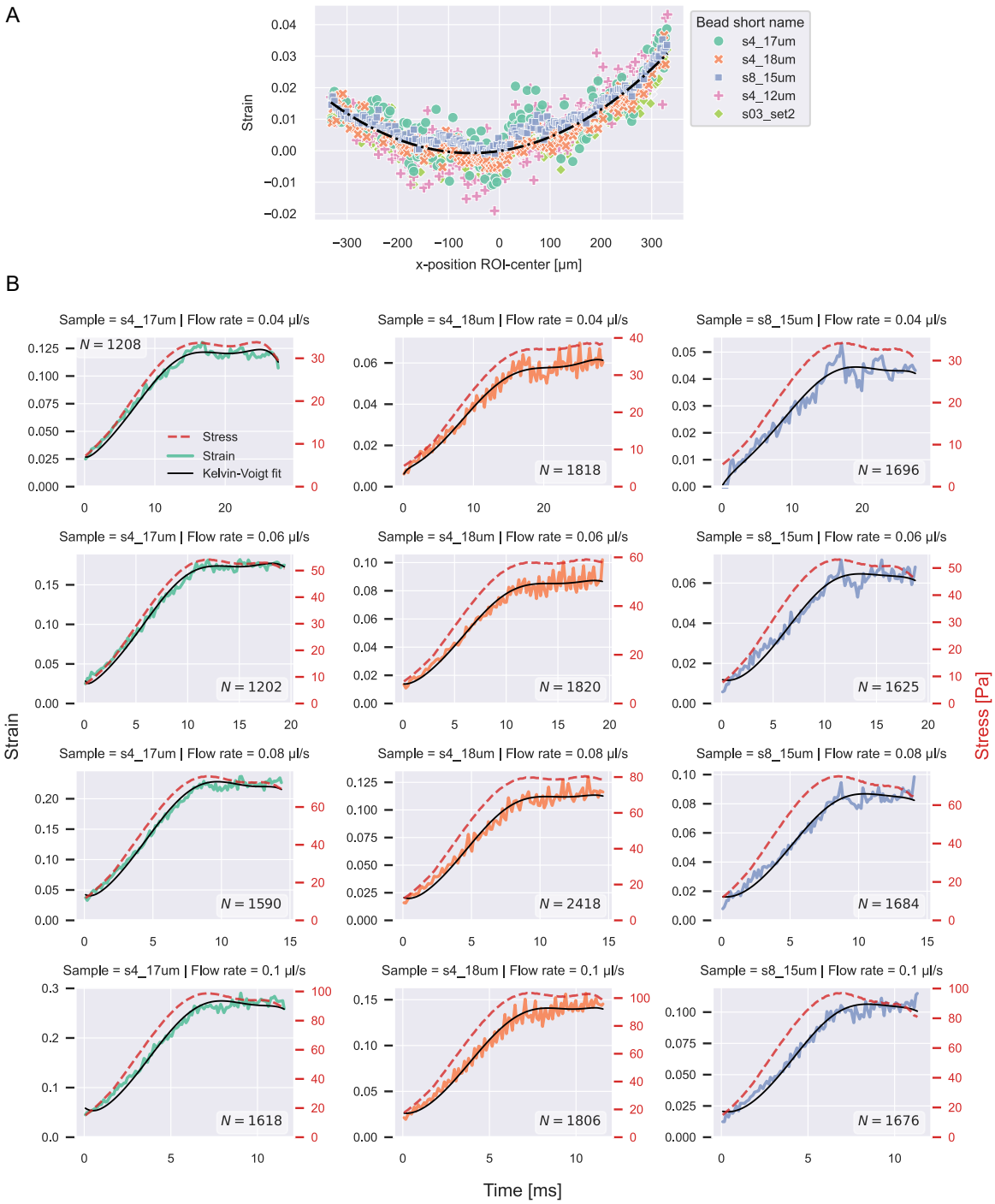

Figure S5: Strains and stresses of PAAm beads. A) Strain of different types of PAAm beads in the inlet region of the channel at a flow rate of 0.01 µL/s. We observed that the correction curve was independent of bead type, size, or stiffness. A quadratic function was fitted with x=0 in the center of the ROI: $\varepsilon = 2.1 \cdot 10^{-7}x^2 + 2.4 \cdot 10^{-5}x - 10^{-4}$ (black dash-dotted line). **B**) Corrected strain curves and stress curves as function of time for all bead experiments in the hyperbolic region. The solid black lines indicate the Kelvin-Voigt fit to the data according to Equation (13). Numbers N indicate the number of beads included per condition.

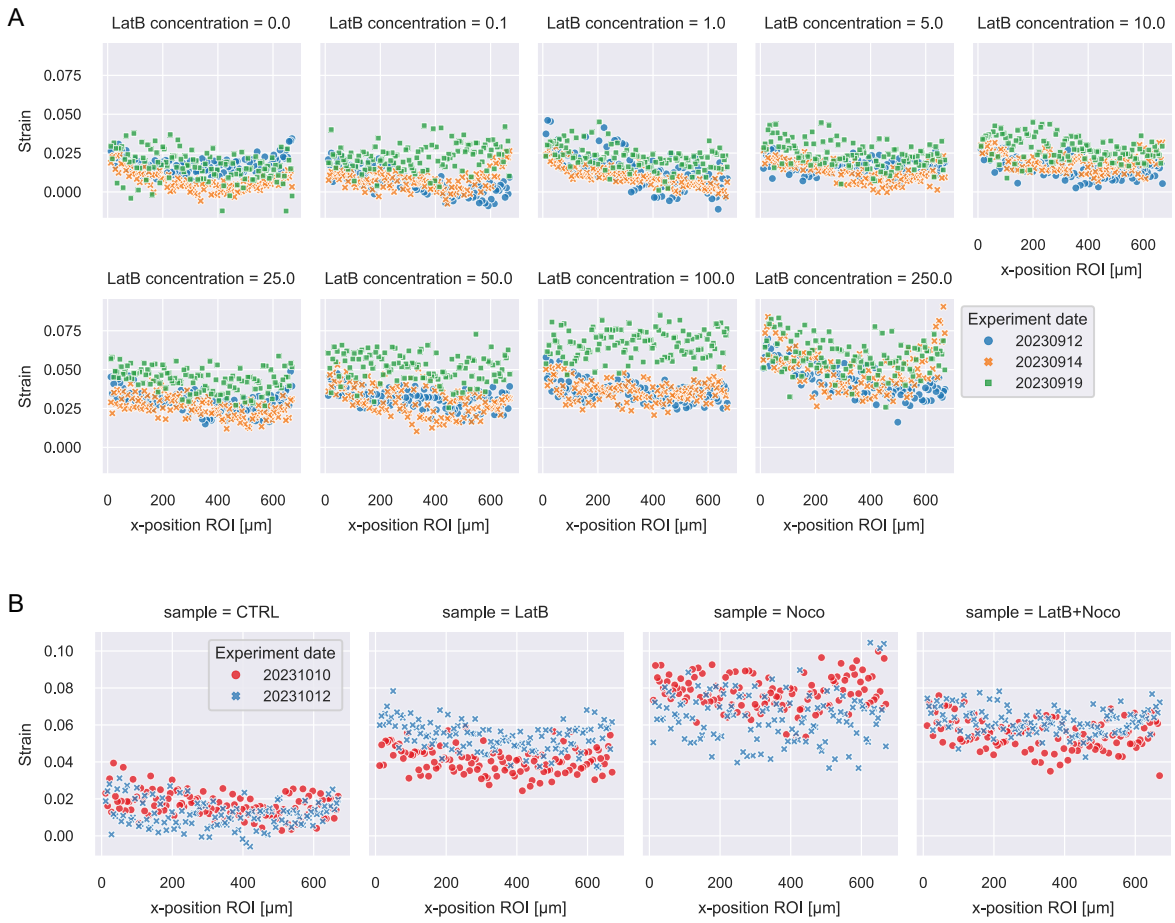

Figure S6: Strains of HL60 cells + treatment in the inlet region. A) Strain curves for all HL60 cell with LatB treatment conditions in the inlet region at a flow rate of 0.01 µL/s. **B**) Same data for cells with LatB + Nocodazole treatment.

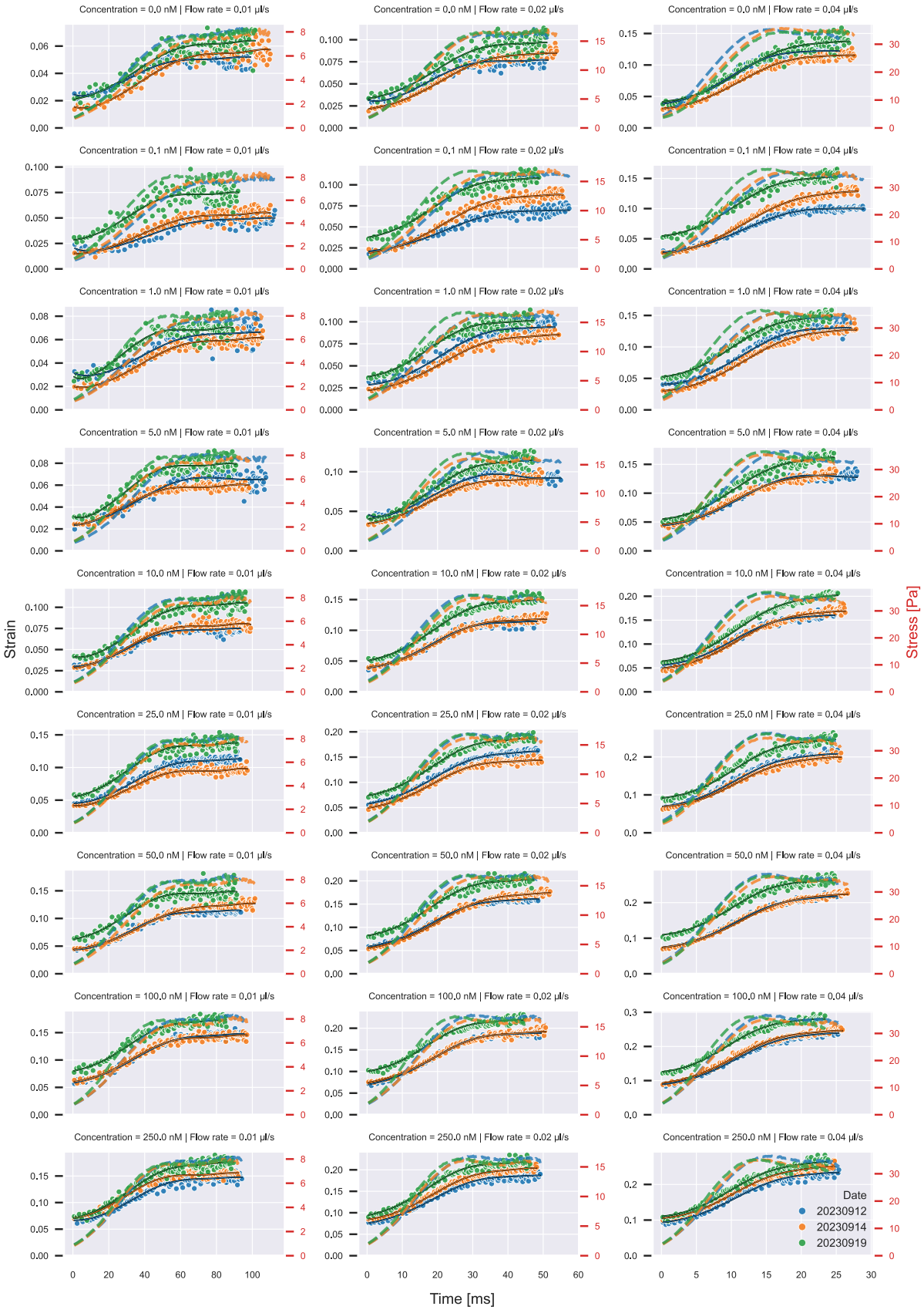

Figure S7: Stress and strain curve as function of time for all HL60 experiments with Latrunculin B treatment. Scatterplots show strain data. Dashed lines show stress curves for the respective experiment. Solid lines show the Kelvin-Voigt fit to the data according to Equation (30).

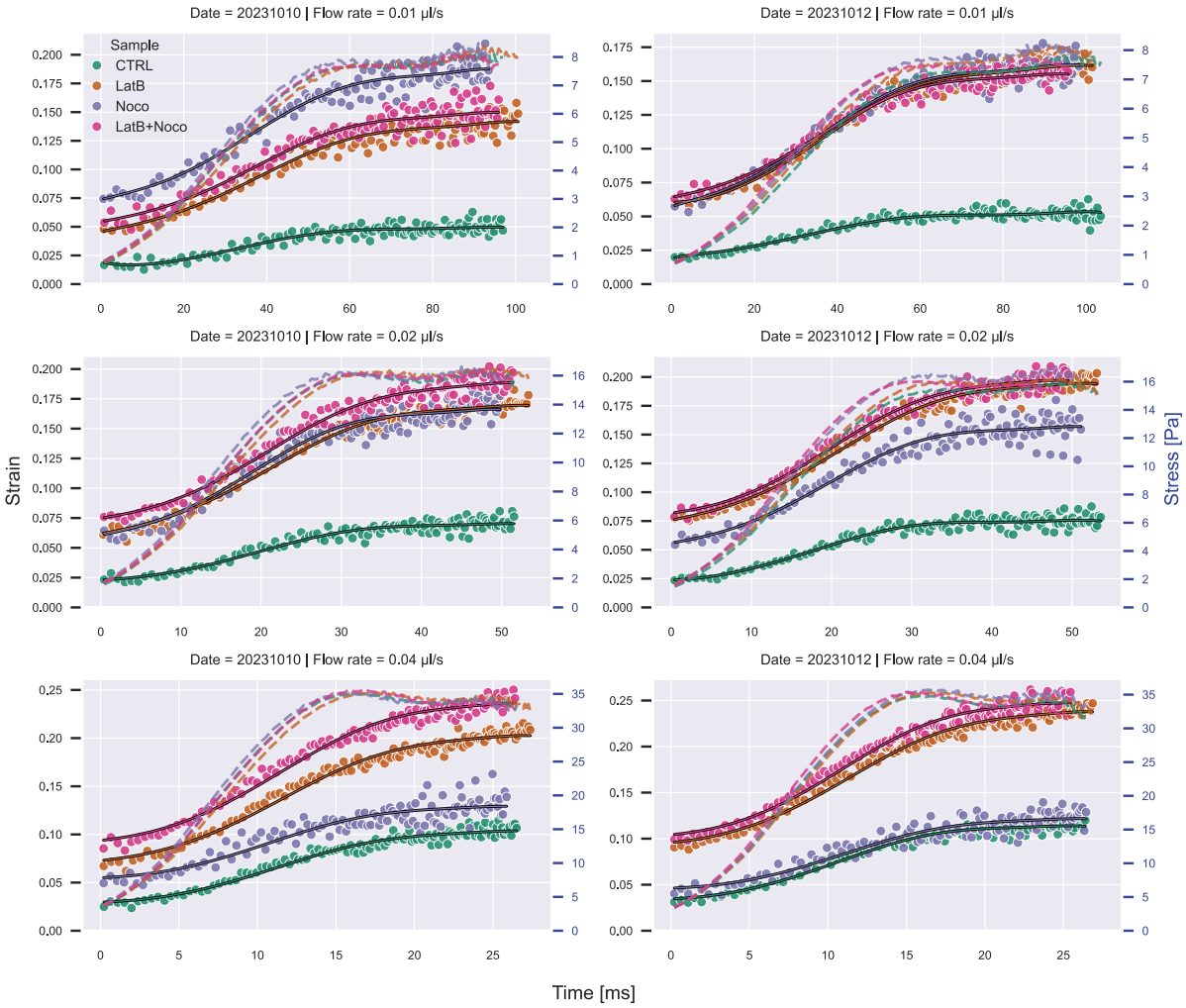

Figure S8: Stress and strain curves as function of time for all HL60 experiments with Latrunculin B and Nocodazole treatment. Scatterplots show strain data. Dashed lines show stress curves for the respective experiment. Solid line show the Kelvin-Voigt fit to the data according to Equation (30).